(4)

THE OHIO STATE UNIVERSITY

AD-A218 212

High Resolution Radar Target Modeling Using ARMA Models

R. Carrière and R. L. Moses

The Ohio State University
ElectroScience Laboratory

Department of Electrical Engineering
Columbus, Ohio 43212

Technical Report 718048-11
Contrct No. N00014-86-K-0202
April 1989

Department of the Navy
Office of Naval Research
800 North Quincy Street
Arlington, Virginia 22217-5000

NOTICES

When Government drawings, specifications, or other data are used for any purpose other than in connection with a definitely related Government procurement operation, the United States Government thereby incurs no responsibility nor any obligation whatsoever, and the fact that the Government may have formulated, furnished, or in any way supplied the said drawings, specifications, or other data, is not to be regarded by implication or otherwise as in any manner licensing the holder or any other person or corporation, or conveying any rights or permission to manufacture, use, or sell any patented invention that may in any way be related thereto.

50272-101

REPORT DOCUMENTATION PAGE	1. REPORT NO.	2.	3. Recipient's Accession No.

4. Title and Subtitle
High Resolution Radar Target Modeling Using ARMA Models

5. Report Date
April 1989

6.

7. Author(s)
R. Carrière and R.L. Moses

8. Performing Org. Rept. No.
718048-11

9. Performing Organisation Name and Address
The Ohio State University
ElectroScience Laboratory
1320 Kinnear Road
Columbus, OH 43212

10. Project/Task/Work Unit No.

11. Contract(C) or Grant(G) No.
(C) N00014-86-K-0202
(G)

12. Sponsoring Organization Name and Address
Office of Naval Research
800 North Quincy Street
Arlington, Virginia 22217-5000

13. Report Type/Period Covered
Technical Report

14.

15. Supplementary Notes

16. Abstract (Limit: 200 words)

A method for characterizing radar signatures using ARMA models is developed based on the concept of scattering centers. A parameterization of the ARMA model specific to the radar target identification problem is chosen, and several key improvements to the algorithm, including the use of singular value decomposition and the removal of spurious scattering centers are presented and compared to earlier versions of the algorithm. The resulting algorithm is tested with data taken from a compact range. These tests include comparison of different targets, different aspect angles and frequency ranges, as well as robustness tests on the algorithm and evaluation of performance in noise.

17. Document Analysis a. Descriptors

b. Identifiers/Open-Ended Terms

c. COSATI Field/Group

18. Availability Statement	19. Security Class (This Report)	21. No. of Pages
A. Approved for public release; Distribution is unlimited.	Unclassified	55
	20. Security Class (This Page) Unclassified	22. Price

(See ANSI-Z39.18) *See Instructions on Reverse* OPTIONAL FORM 272 (4-77)
Department of Commerce

Contents

List of Figures

List of Tables

1. Introduction

The original goal of radar (radio detection and ranging) was to provide information about the existence and position of targets. It was soon realized that additional capabilities were desirable, in particular the ability to classify the target. Depending on the nature of the application, classification might be concerned with friend or foe status or with flight rule status (visual/instrumental) or many other things. In some cases it is possible to obtain this information by requiring the aircraft to transmit it via transponders or IFF devices; in other cases this is impossible or undesirable. The latter problem is the so called non-cooperative radar target identification (RTI) problem.

From physical considerations it is known that information about the shape of the target is present in the radar return signal, since the target will distort the incoming radar signal in a geometry-dependent manner. The problem of RTI is to extract useful information from the distortions in the radar return. This extraction process can be considered to consist of two stages: first there is a signal processing stage, where the radar return signal is processed to extract some discriminating information; second is the decision stage, where the extracted information from the signal processing stage is matched against a data base of known targets (the catalog), and a decision as to the nature or identification of the target is made.

One method of performing target identification is to use no signal processing step, so the decision algorithm operates directly on the frequency data. This method has the advantages of simpler implementation and of not losing information in the signal processing stage. However, there are some potential disadvantages. First, if the number of frequency measurements is large, the decision step will be computa-

tionally intense. Second, the frequency domain information does not relate to the geometric configuration of the target in a direct manner; thus, one cannot directly obtain geometric information, such as overall length, about the target.

This report considers an alternative approach to target identification. In this approach, the signal processing step is designed to extract geometrically relevant scattering characteristics of the target. This method of RTI consists of a signal processing step which converts the radar return from the frequency to the time domain, to obtain the radar cross-section versus time signal of the target. The advantage of this method is that the relation with the geometry of the target is much more direct in this representation. The decision step then classifies the target from the time domain information. Traditionally the transition to the time domain has been accomplished using Fast Fourier Transform (FFT) techniques [1]. FFT techniques suffer from two potential disadvantages, however. First, they do not yield any data reduction, so the output of the signal processing stage gives at least as many data points in the time domain as originally present in the frequency domain. Thus, there is no decrease in processing requirements for the decision algorithm. Second, the time resolution of the FFT is limited by the bandwidth of the frequency domain return, so closely spaced features on the target might not be resolved.

This report addresses the option of using modern signal processing methods to convert from the frequency to the time domain. In particular, Autoregressive Moving Average (ARMA) models are used to parameterize the radar data. ARMA models do not suffer from the resolution limit of the FFT methods. In addition, ARMA models are parametric, so the information present in a large number of frequency samples can be concentrated into a small number of parameters, thus

reducing the computational burden for the decision stage. Finally, the parameters in the ARMA model are closely related to relevant geometric features of the target. As a result, even if the target cannot be identified, some geometric information about the target can be extracted from the ARMA parameters.

In this report, we study the application of ARMA models to the signal processing part of the RTI problem. First, we develop a special representation for the ARMA model suited to the specifics of the RTI problem. We then describe an algorithm for estimating the needed parameters from the frequency data. We study the effects of several improvements over the basic algorithm, including the use of singular value decomposition and the elimination of spurious scattering centers from the estimated model. Both lead to an algorithm that is more robust. Finally, we present results of this algorithm are shown using radar data obtained by compact range measurements of commercial aircraft models.

2. Canonical Scatterers and ARMA Models

This chapter discusses the modeling of radar targets by canonical scattering centers, and the relation to ARMA models. In particular, it will be shown that ARMA models are an appropriate way of modeling radar returns.

2.1 Canonical Scatterers

It is well-known [2] that scattering of electromagnetic waves at high frequencies, i.e. at frequencies such that the wavelength is small compared to the scatterer, can be modeled as a set of independent scattering centers. There are several varieties of canonical scattering centers used in this process; typical examples are [2] the point, edge and plate scatterers and the corner reflector. As is stated in [2], these examples are typical of the types of scatters that can be found on radar targets.

From [3], we have that all the above canonical types of scatterers can be modeled in the following way: if a target consisting of m scatterers is illuminated using a CW radar, then the backscattered field received by a linearly polarized antenna will give a signal of the form:

$$y_k = \sum_{i=1}^{m} K_i e^{\frac{-j2r_i 2\pi f_k}{c}} (j2\pi f_k)^{t_i} \tag{2.1}$$

where K_i is the amplitude, r_i the relative range, and t_i the type of the i^{th} scatterer; f_k is the k^{th} frequency, and m is the number of scatterers. For the canonical scatterers in [3], t_i takes on the following values

$$t_i \in \{-1, -0.5, 0, 0.5, 1\} \tag{2.2}$$

In addition, for stepped frequencies, we can represent f_k by

$$f_k = f_0 + k\delta_f, \quad k = 0, 1, 2, \ldots, N-1 \tag{2.3}$$

where f_0, δ_f and N are given parameters of the system under consideration. The frequency f_0 represents the lowest frequency the radar system transmits and δ_f is the size of the frequency step. Estimation of the parameters in (2.1) from N measurements leads to a canonical scattering description of the target; see [3]. Unfortunately, this estimation is nonlinear, and is not practical for real-time target identification at this time.

For reasonably small bandwidths, a feasible method of target identification can be obtained by approximating the canonical scattering model of (2.1). In particular, the factor $(j2\pi f_k)^{t_i}$ can be approximated by a factor of the form ρ_i^k for some ρ_i. This approximation yields the data model:

$$y_k = \sum_{i=1}^{m} d_i p_i^k \tag{2.4}$$

where d_i is in general not equal to K_i in (2.1) because of the approximation involved. The variable p_i can be found from:

$$p_i = \rho_i e^{-j\frac{2r_i 2\pi f_k}{c}} \tag{2.5}$$

or, conversely, we can find ρ_i and r_i from p_i by:

$$\rho_i = |p_i| \tag{2.6}$$

$$r_i = (\frac{1}{2} - \frac{\arg p_i}{2\pi})R \tag{2.7}$$

where $R = \frac{c}{2\delta_f}$ is the maximum unambiguous range of the radar. In practice the absolute range is not used; instead, r_i represents the range relative to a zero range

reference point.

The physical relevance of the ρ_i parameter is dubious because it is defined from an approximation. However, it is important to estimate ρ_i since it allows the calculation of a physically important quantity: the amount of energy associated with a scattering center. This energy can found by considering the contribution of a single scattering center to the total signal. The single scattering center component is

$$\{d_i p_i^k\}_{k=0}^{N-1}$$

The energy is the square of the absolute value of this contribution, or

$$P_i = \sum_{k=0}^{N-1} |d_i|^2 |p_i|^{2k} = |d_i|^2 \frac{1-\rho_i^{2N}}{1-\rho_i^2} \tag{2.8}$$

Equations (2.4) and (2.8) will be used to form a parametric model of target scattering.

2.2 The ARMA Modeling Interpretation

In the previous section we established that the return of a stepped frequency radar can be modeled as

$$y_k = \sum_{i=1}^{m} d_i p_i^k$$

In this section we will show how this relates to Autoregressive Moving Average (ARMA) modeling and the radar cross section versus time relation of the target.

If we take the inverse Fourier Transform of the above relation for y_k, we get

$$Y(r) = \sum_{i=1}^{m} \frac{d_i}{e^{j\pi(1-2r/R)} - p_i}, \quad 0 \le r \le R \tag{2.9}$$

where r is relative range. The square of the absolute value of this function gives the radar cross section as a function of relative range.

If we change from the Fourier to $\mathcal{Z}$ Transform (i.e. $z = e^{j\pi(1-2r/R)}$), equation (2.9) becomes

$$Y(z) = \sum_{i=1}^{m} \frac{d_i}{z - p_i} = \frac{C(z)}{A(z)} \tag{2.10}$$

where

$$A(z) = \prod_{i=1}^{p} (z - p_i) = z^p + a_1 z^{p-1} + \ldots + a_p \tag{2.11}$$

and where $C(z)$ is a polynomial of degree less than or equal to $m - 1$. It can be seen that the p_i coefficients are the zeros of $A(z)$, and so they are the the poles of $Y(z)$. Hence the model we have assumed for the radar data corresponds to an autoregressive moving average model with m poles and $m - 1$ zeros.

Note that the exponential model (2.4) applies to the frequency domain, and the rational model (2.9), (2.10) applies to the time domain. This is in contrast to standard time series analysis treatments of ARMA models, where the damped exponential model applies to the time domain, and the corresponding rational transfer function model is in the frequency domain [4]. This difference is cosmetic only, and is easily handled.

Comparing (2.4) with (2.10), it can be seen that each term $\{d_i p_i^k\}_{k=0}^{N-1}$ corresponds to a term $\frac{d_i}{z-p_i}$. As has been stated above, the terms $\{d_i p_i^k\}_{k=0}^{N-1}$ correspond to the scattering centers of the target; hence, the $\frac{d_i}{z-p_i}$ terms model the response of the individual scattering centers in the time domain. In other words, the time domain model (2.10) describes the radar cross section (RCS) versus time response of the target as the sum of the RCS responses of the scattering centers. The RCS time response can be obtained by evaluating (2.9) for $0 \leq r < R$ or equivalently,

evaluating (2.10) for $z = e^{j\phi}$, $0 \leq \phi < 2\pi$. This RCS time response is similar to the responses obtained by taking the DFT of the frequency data, but does not have the resolution limitation inherent in the DFT.

The nature of each scattering center is determined by the values of the parameters $p_i = \rho_i e^{j\pi(1-2r_i/R)}$ and d_i associated with it. First, r_i determines the relative range. Second the magnitude ρ_i of p_i determines the shape of the RCS response curve; if ρ_i is close to one (i.e. p_i is close to the unit circle), the curve will be a narrow and sharp peak, indicating that the scattering is concentrated at a particular range. If on the other hand, ρ_i is not close to one (i.e. p_i is far away from the unit circle), the curve is much wider and has no sharp peak, indicating the scattering center response is spread out in range. Finally, the values of ρ_i and d_i combine to give the energy P_i associated with the scattering center, as indicated in (2.8).

The above ideas are illustrated in Figure 2.1. This Figure shows the response $|Y(r)|$ of a hypothetical target composed of four scattering centers. The lower graph shows the location of the zeros $\{p_i\}_{i=1}^4$ in the complex plane. By comparing the locations of the zeros and the positions of the peaks in the response graph, we can clearly see how the argument of p_i relates to the range of the corresponding peak. Also, by comparing peaks 3 and 4, we can see that when p_i is closer to the unit circle, the corresponding peak will be sharper and narrower. Peaks 1 and 2 show that even if two scattering centers have p_i's that are equally close to the unit circle, the amplitude of their peaks may vary greatly, since the d_i values may be different. For reference, Figure 2.2 shows the FFT of the same hypothetical target.

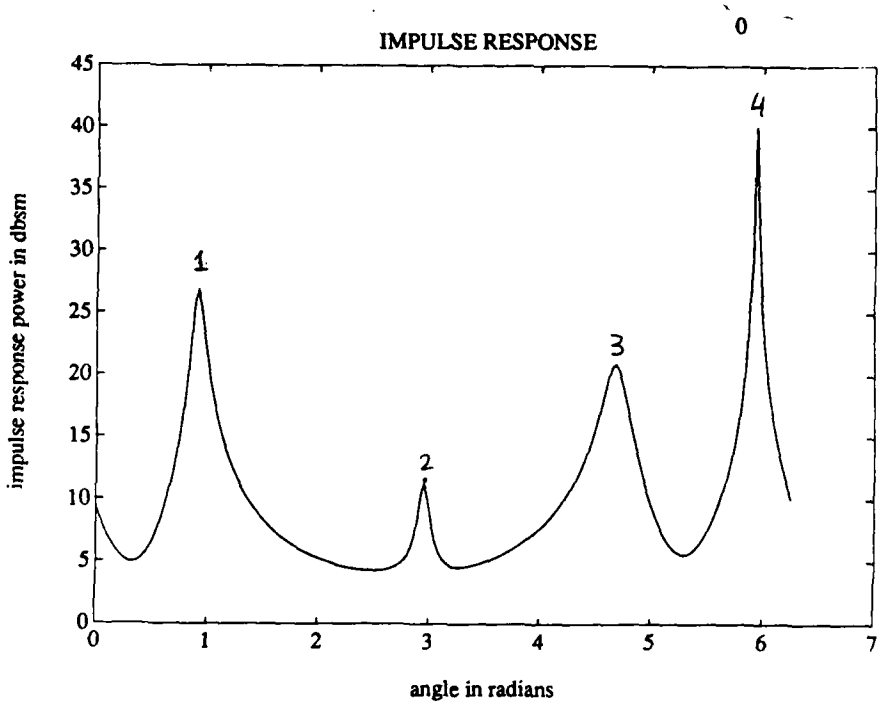

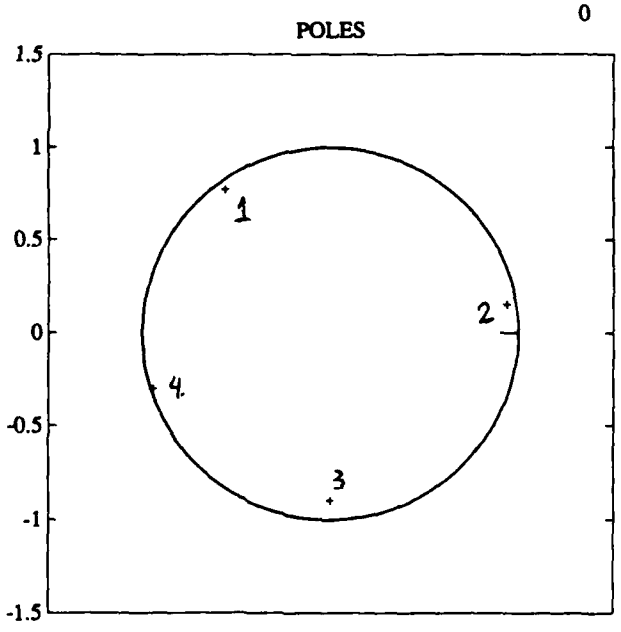

Figure 2.1: Response and Z-plane for a Hypothetical Target.

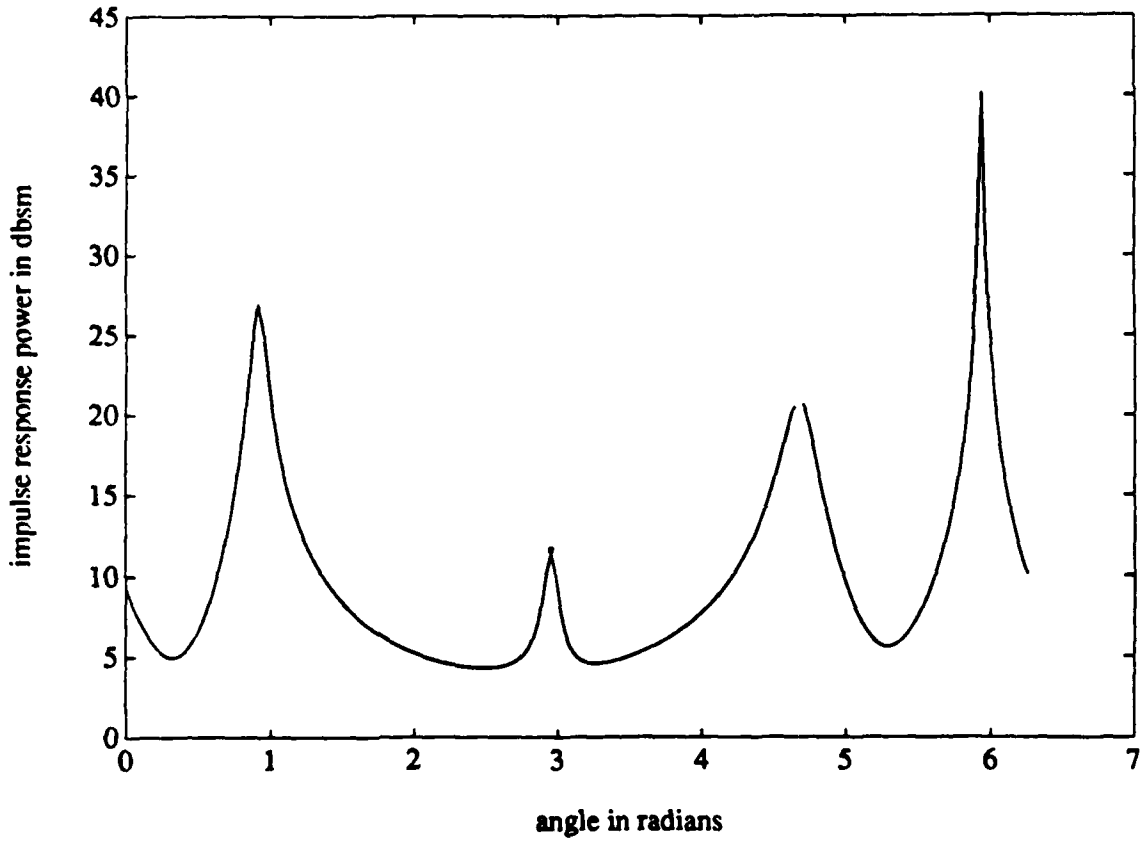

Figure 2.2: FFT for the Hypothetical Target.

3. Techniques to Estimate the Model Parameters from Radar Data

Based on the results of the previous section, the frequency domain radar backscatter data can be modeled as a sum of complex exponential terms. More practically, the data will also contain an additive noise component due to receiver noise, clutter, etc. In either case, the signal processing objective is to estimate the parameters which describe the exponential components from a finite set of (possibly noisy) data. This problem is considered in the time series analysis literature as the so-called Prony estimation problem [4].

Below, we develop algorithms which estimate the needed parameters from radar data. These algorithms are based on singular value decomposition (SVD) versions of Prony algorithms. We then discuss modifications to the algorithms to make them more appropriate for radar data.

3.1 The Backward Prediction Equations

Assume that we wish to model the radar data as a sum of complex exponentials, as in equation (2.4), and that the measured data contains noise: thus

$$y_k = \sum_{i=1}^{m} d_i p_i^k + n_k, \quad k = 0, \ldots, N-1 \tag{3.1}$$

where $\{n_k\}_{k=0}^{N-1}$ is a sequence of zero mean noise. For concreteness, we will assume n_k is white noise with zero mean and variance λ^2; however, the colored noise case can also be handled, using algorithms similar to the ones we describe below [5]. Below we discuss various alternative ways to estimate the p_i and d_i coefficients from the measured data sequence $\{y_k\}_{k=0}^{N-1}$. These methods are adapted from similar algorithms discussed in [4].

First we consider the estimation of the p_i parameters. Recall that the p_i parameters are the zeros of the $A(z)$ polynomial (see equation (2.10)). It can be shown [4] that the coefficients a_i of the $A(z)$ polynomial satisfy the equation:

$$y_k + \sum_{i=1}^{m} a_i y_{k+i} = 0$$

This can be written in matrix form as:

$$\begin{bmatrix} y_{M+1} & y_M & \cdots & y_1 \\ y_{M+2} & y_{M+1} & \cdots & y_2 \\ \vdots & \vdots & \ddots & \vdots \\ y_{N-1} & y_{N-2} & \cdots & y_{N-M-1} \end{bmatrix} \begin{bmatrix} a_M \\ \vdots \\ a_1 \\ 1 \end{bmatrix} \approx 0 \qquad (3.2)$$

Where M is some integer at least equal to m and where equality holds in the noiseless case; we will discuss the selection of M below. Solutions based on (3.2) are called total least squares solutions [6]. It was shown in [6] that total least squares solutions generally have superior accuracy when compared with ordinary least squares methods [6].

It should be noted here that in a given application we would not know the correct value of m. This point will be further discussed below.

3.2 Use of the Singular Value Decomposition

Estimation of parameters from a short data record is a difficult problem; while most popular techniques are quite good at estimating parameters from noisy data if the record length is large, their ability to perform well for short records is significantly less. One technique modern signal processing research has found to combat this effect is the use of the Singular Value Decomposition (SVD). The SVD is an

orthogonal decomposition technique for matrices; it can be regarded as a generalization of the eigenvalue decompositions that exist for square matrices.

The use of the SVD to the estimation problem lies in its ability to help determine the rank of a noisy matrix. Recall that estimating the polynomial $A(z)$ requires forming a matrix out of the noisy data (equation (3.2)). In the noiseless case, the rank of this matrix is m, the number of scattering centers on the target. However, due to the effect of the noise on the data, the actual rank will be greater than m. For small noise variances, the data matrix will be "close" to a matrix of rank m, and the SVD can help find the closest rank m approximation. It is expected that this procedure will reduce the effects of the noise on the estimate. For a more detailed discussion, see [7,8,9].

Next we need to consider how to implement the SVD technique in our algorithm. To do this we modify equation (3.2) as follows: we first compute the matrix on the left of (3.2) and then compute its SVD:

$$Y = U\Sigma V^H \tag{3.3}$$

where Y is the data matrix, U and V are unitary matrices, and Σ is a diagonal

matrix, given by:

$$\Sigma = \begin{bmatrix} \sigma_1 & 0 & \dots & 0 \\ 0 & \sigma_2 & \dots & 0 \\ \vdots & \vdots & \ddots & \vdots \\ 0 & 0 & \dots & \sigma_{M+1} \\ 0 & 0 & \dots & 0 \\ \vdots & \vdots & \ddots & \vdots \\ 0 & 0 & \dots & 0 \end{bmatrix}_{(N-M-1)\times(M+1)} \tag{3.4}$$

where

$$\sigma_1 \geq \sigma_2 \geq \ldots \geq \sigma_{M+1} \geq 0. \tag{3.5}$$

As noted above, if the SNR is sufficiently high, we will have:

$$\sigma_1 \geq \ldots \geq \sigma_m \geq \sigma_{m+1} \geq \ldots \geq \sigma_{M+1} \tag{3.6}$$

where $\sigma_{m+1} \ldots \sigma_{M+1}$ are nonzero only because of the nonzero noise term. Thus, some effects of the noise can be eliminated by replacing Σ by Σ' defined as

$$\Sigma' = \begin{bmatrix} \sigma_1 & & & 0 \\ & \ddots & & \\ & & \sigma_n & \\ 0 & & & 0 \end{bmatrix}_{(N-M-1)\times(M+1)} \tag{3.7}$$

for some value of n satisfying $m \leq n \leq M+1$ (we will discuss ways of choosing n below). Finally, the vector $\hat{a} = [1\hat{a}_1 \ldots \hat{a}_M]^T$ is found by solving

$$U\Sigma' V^H \hat{a}_M = 0 \tag{3.8}$$

in the least squares sense [6].

The SVD also greatly helps the order estimation problem. Assume we do not know the true number of scattering centers m, but are confident that the value of M is large enough to model the scattering behaviour of the target. Then we can select $n \leq M$ to best model the target and reject noise. Given the short data lengths typical of RTI problems, a large enough M can typically be achieved by choosing M to be a large fraction of, or even equal to, $\frac{N}{2}$. Then n can be chosen by considering the distribution of the sv's: we choose n such that σ_{n+1} is the first sv that falls below a preset threshold. In this way $\sigma_1 \ldots \sigma_n$ represent the important (high energy) signal components, and the other sv's represent either small signal components or noise. Note that we may not model all of the target scattering components, as the weaker ones can be eliminated from the model by choosing n small; on the other hand, the weaker scattering components are more prone to be misestimated in noise. Thus, this procedure represents a trade-off between geometric faithfulness and robustness in the presence of noise. The clear advantage of this method is its built-in robustness: it selects the high energy signal components, which are expected to suffer the least degradation from the noise. Another advantage of this method over order selection in a straightforward, non-SVD estimator is that because the order reduction proceeds in an orthogonal manner, we do indeed select the strongest signal components, whereas the straightforward algorithm will select mixtures of several components, as can be seen from the experiments in [10]. The SVD method is one of the best currently known practical methods for tackling the order estimation problem for radar data.

3.3 Estimation of Modal Amplitudes

Once we have estimates of the $A(z)$ polynomial coefficients, we can find the corresponding zeros p_i by using a polynomial root finding method. It then remains to find the corresponding amplitude (d_i) coefficients. From equation (2.4) we can see that given the p_i, the problem of estimating the d_i is a linear one, so we can use a standard Least Squares approach. Of course we do not know the correct values of the p_i, but we can use the estimates obtained as described above in their stead. The least squares approach to estimating the d_i coefficients can be formulated as follows:

$$\begin{bmatrix} \hat{p}_1^0 & \cdots & \hat{p}_M^0 \\ \vdots & & \vdots \\ \hat{p}_1^{N-1} & \cdots & \hat{p}_M^{N-1} \end{bmatrix} \begin{bmatrix} \hat{d}_0 \\ \vdots \\ \hat{d}_{N-1} \end{bmatrix} - \begin{bmatrix} y_0 \\ \vdots \\ y_{N-1} \end{bmatrix} \approx 0 \tag{3.9}$$

where $\hat{p}_i$ are the estimates obtained from the first step. This equation is simply (3.1) written out in matrix form. Since the equation (3.9) is overdetermined, we can solve it in a least squares sense.

3.4 Elimination of Spurious Zeros

In previous sections we computed an estimate of a polynomial $A_M(z)$ of order $M > m$, and a corresponding set of M zeros $\{p_i\}_{i=1}^M$. We also computed amplitudes corresponding to these zeros. The next step is to separate the m zeros that correspond to the radar target (signal zeros) from the remaining spurious zeros.

In [10], we reported a criterion for zero inspection that worked well with a related ARMA algorithm. This criterion is based on the observation that a zero with modulus greatly different from one will influence only the data elements at the

start (if the modulus is smaller than one) or at the end (if it is greater than one). In the time domain, we observe that such zeros correspond to widely distributed scattering centers, which are of little interest to radar target identification. As reported in [10], removal of such zeros improved the performance of the algorithm we were then using.

Unfortunately, the criterion in [10] does not seem to mesh well with the current SVD-based algorithm. Results of applying this zero selection method on aircraft data shows two undesirable characteristics. First, this criterion produces erratic changes in the selected zeros as one changes the value of m. This is undesirable for RTI applications because our experience has shown that one needs to select the order differently for different aircraft. Therefore, it is necessary for the order to be selected on-line, and thus we need algorithms that will produce similar estimates even if the order selected for the noisy data differs from the order selected for the catalog prototype. Second, the experimentally found spread of the resulting d_i and ρ_i parameters was such as to make them useless for classification: there were no clear clusters for the different targets. Hence, we needed a better way to differentiate spurious zeros from the signal zeros. We are currently investigating two different techniques, as detailed below.

The first technique is a refinement of the method in [10]. Whereas in [10] we kept all zeros within an ring around the unit circle with outer radius r and inner radius $\frac{1}{r}$, we now choose the outer and inner radii of the ring independently. In particular, since one expects spurious zeros to lie inside the unit circle when using backward prediction equations [4], the inner radius is set much closer to the unit circle than the outer one.

The second technique relies on the observation that since the spurious zeros correspond to modes that are not present in the data, their estimated energy should be low. To take advantage of this property, the algorithm is modified as follows. First, all M zeros are kept, and the amplitudes $\{d_i\}_{i=1}^{M}$, corresponding to those zeros are found using equation (3.9). Then, the energy of each mode is computed using equation (2.8). The m zeros whose corresponding energy is the highest are kept and the remaining ones are discarded. Then, the energy estimates for the m kept zeros can be refined by recomputing the amplitude estimation using (3.9) with only the m selected zeros, however, since the energies for the discarded zeros is low, the difference between the two estimates should generally be small, so this refinement step may be omitted.

Preliminary simulation results indicate that the zero selection technique which uses the energy criterion performs significantly better than the one using zero radii. This will be seen in the experiments presented in section 4.

Table 3.1 summarizes the ARMA modeling algorithm used in this report.

3.5 Classification Aspects [1]

In this section we report results pertaining to experiments we performed to get more insight into the ability of the algorithms discussed to form the signal processing stage before a classifier. We have looked at the experimentally found distribution function for the distance of the two strongest scattering centers on a Boeing 747, at the clustering properties of the ρ_i and d_i parameters, and at the residual error (defined below) as a function of n.

[1]The authors would like to thank O.S. Sands for his contributions to this material.

Table 3.1: Summary of the Algorithm.

1. Find the zeros $\{p_i\}_{i=1}^{M}$ from the frequency data $\{y_k\}_{k=0}^{N-1}$ as follows:

   (a) Given M, form the matrix Y in (3.2) and obtain a singular value decomposition of Y as defined (3.3).

   (b) Given a cutoff criterion, find the smallest n such that σ_n satisfies the criterion, but σ_{n+1} does not. Now solve the equation

   $$U\Sigma' V^H \hat{a}_M = 0$$

   for $\hat{a}_M$, where U, Σ' and V are defined in (3.3), (3.7) and (3.8).

   (c) Find the zeros $\{\hat{p}_i\}_{i=1}^{M}$ of the polynomial $A_M(z)$.

2. Find the modal amplitudes $\{\hat{d}_i\}_{i=1}^{M}$ and energies $\{\hat{P}_i\}_{i=1}^{M}$ associated with $\{\hat{p}_i\}_{i=1}^{M}$ from equations (3.9) and (2.8)

3. Select the m zeros with the highest energies $\hat{P}_i$. From these m zeros $\{p_i\}_{i=1}^{m}$ compute the ranges $\{r_i\}_{i=1}^{m}$ and dispersions $\{\rho_i\}_{i=1}^{m}$ using equations (2.7) and (2.6). Optionally recompute the m amplitudes and and m energies from equations (3.9) and (2.8) using the m selected zeros.

4. The target response $Y(r)$ can be found from (2.9) using the coefficients $\{r_i, \rho_i, d_i\}_{i=1}^{m}$.

The distribution of the difference in relative range between the two scattering centers with the highest energies (i.e. $r_1 - r_2$) for the Boeing 747 in 5 dBsm noise is clearly Gaussian to good approximation in the case of the algorithm as presented in Table 3.1, and it is clearly not Gaussian for the case of the algorithm with the ring criterion described in the previous section (see Figure 3.1). Moreover, in the former case the variance is lower. This is important because it is easier to design classifiers for parameters with a Gaussian distribution than for for other parameters. The most important point however, is that the ring criterion algorithm shows significant bias, whereas the algorithm as presented in Table 3.1 does not. The algorithm as presented in the table gives a mean value for $r_2 - r_1$ that corresponds to the relative range found in the noiseless case; as can be seen from Figure 3.1, the ring algorithm gives a mean that differs from the true mean by more than 10%.

It has further been found that the values of the d_i and ρ_i coefficients tend to cluster in different places in the $d \times \rho$ plane for the different aircraft; this means that these parameters carry information that will aid classification.

Finally, we have found that for the ring criterion algorithm the residual error is not a monotonic function of the number of singular values. The residual error is defined as:

$$E_{res(m)} = \sqrt{\frac{\sum_{k=0}^{N-1}(y_k - \sum_{i=1}^{m} d_i p_i^k)^2}{\sum_{k=0}^{N-1} y_k}} \tag{3.10}$$

It is a measure of how well the estimate models the data. It is known that without the elimination of spurious zeros, $E_{res(m)}$ will decrease monotonically as a function of the number of singular values kept, n. This is an important property, since it guarantees that increasing the number of singular values can only improve the quality of the model. It was found experimentally however, that the ring criterion

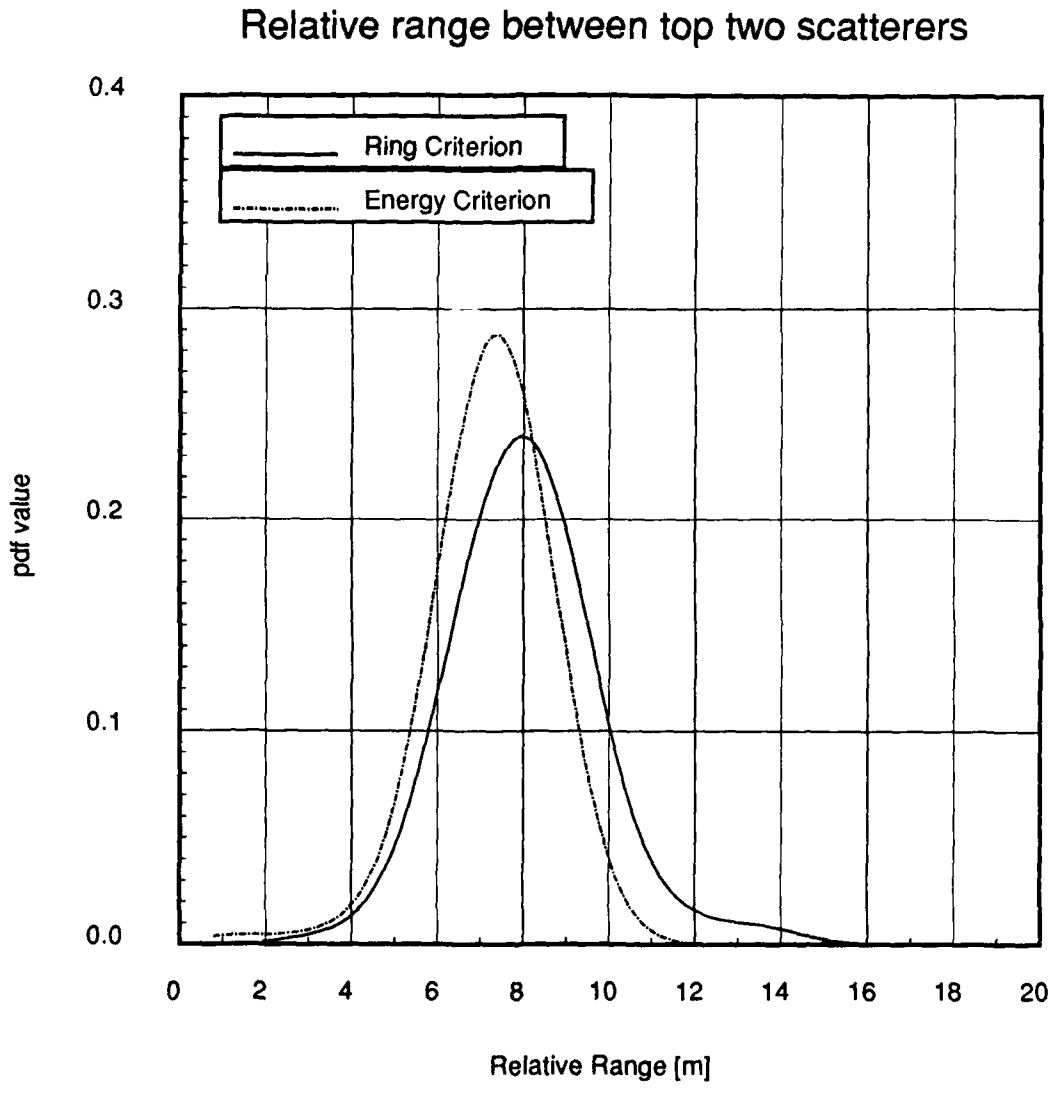

Figure 3.1: Relative Range between the the two strongest scatterers on a Boeing 747, using 20 data points from 6.25–12 GHz, 10th order model, 7 sv's kept.

algorithm did not have this property. In fact, for this algorithm there was no predictable regularity to the error versus singular values function. For the purposes of RTI, it is important that spurious zeros be eliminated, so as to avoid confusing the classifier with physically irrelevant data. It was for this reason that we started to investigate the energy based criterion for keeping zeros, and indeed, we found that for the algorithm presented in Table 3.1, the residual error is a monotonically decreasing function of the number of singular values kept, as desired.

4. Estimation Results Using Compact Range Data

This section describes the results of the signal processing procedure detailed in the previous section when applied to compact range measurements of targets. The data used contain stepped frequency measurements of models of various commercial aircraft; specifically the DC 10, the Concorde and the Boeings 707, 727 and 747 are compared. The measurements have all been made at the OSU ElectroScience Laboratory Compact Range, and are available in various frequency ranges from 2–36 GHz. The size scales for the model aircraft range from 130–200, so the frequencies correspond to the 5–280 MHz for a full-size aircraft, depending on the scale of the of the aircraft under consideration.

The stepped frequency measurements consist of amplitude and phase of the radar return from the target at each frequency. The radar receiver hardware range gates the returning signal to eliminate spurious scattering effects from the anechoic chamber. The data is then calibrated by subtracting the return of the empty chamber (with pedestal) and dividing by the calibrated return for a reference target. The calibrated measurements obtained are then essentially error-free [11]. For those experiments where we have used noisy data, we have added white Gaussian noise to these measurements.

4.1 Tests of Sensitivity to Parameter Selection

First we look at the sensitivity of the ARMA algorithm with respect to choices of certain parameters in the algorithm, such as model order M, number of singular values kept n, etc. We also consider this sensitivity for the two methods of zero

selection as described in Section 3.4. We first show the algorithm sensitive to parameter selections when a radius test is used for zero selection.

If the radius test method is used (see Section 3.4), then Step 3 in Table 3.1 is not performed, and instead in Step 1c the value m is determined as the number of zeros that fall within a preset ring of inner radius $r_1 < 1$ and outer radius $r_2 > 1$. These m zeros are selected and all following steps are performed with only this subset of zeros. This implies that all subsequent steps use m instead of M.

Figure 4.1 shows the estimated response for the Concorde model, using model frequencies from 18 to 26 GHz (this corresponds to frequencies from 138–200 MHz on the full-size Concorde), $N = 30$ data points, an order $M = 10$, while keeping $n = 5$ singular values and $m = 2$ zeros. The same figure also shows a response curve that corresponds to the same situation except that only 3 sv's are kept in the estimate. For reference, the FFT of the Concorde data is shown Figure 4.2. This figure shows the absolute value (in dB) of the inverse Fourier Transform of the data used by the algorithm. The inverse Fourier Transform has been evaluated by zero padding the 30 data points to 512 and taking the IFFT. It is clear that the ARMA algorithm is sensitive to changes in the number of singular values kept. Similar observations can be made for the number of zeros kept and the model order. This verifies the claim that the ring method of zero selection is sensitive parameter choices. The figure given is a typical case taken out of a large number of trials that we have performed.

If, on the other hand, we use energy as the criterion for keeping zeros (that is, if we use the algorithm as presented in Table 3.1) we obtain the responses in Figure 4.3 where we have the same frequency data as before, but now we use a

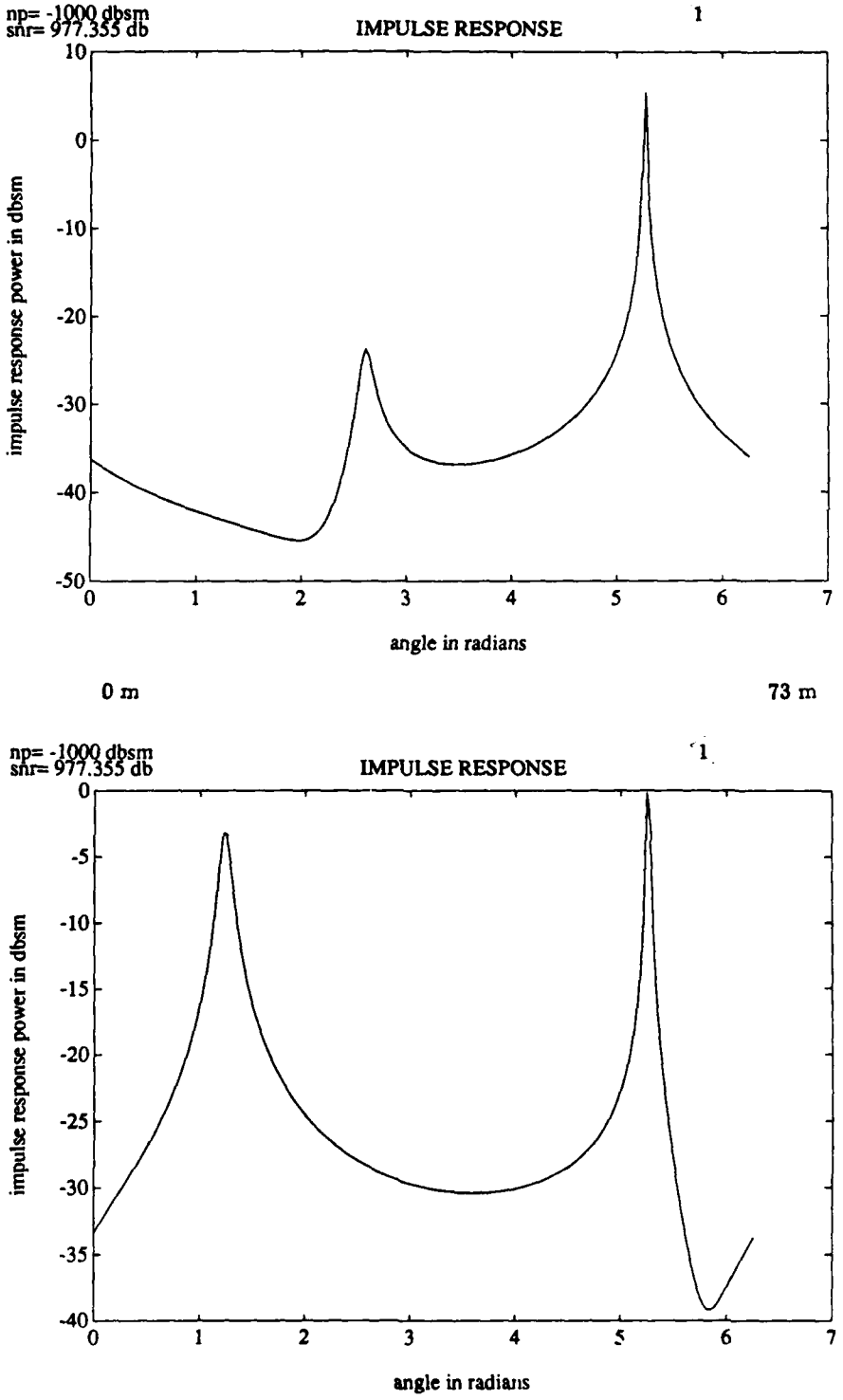

Figure 4.1: Concorde, 18-26 GHz, 10th order model, 5 and 3 sv's kept, 2 zeros kept, 0 degree aspect angle.

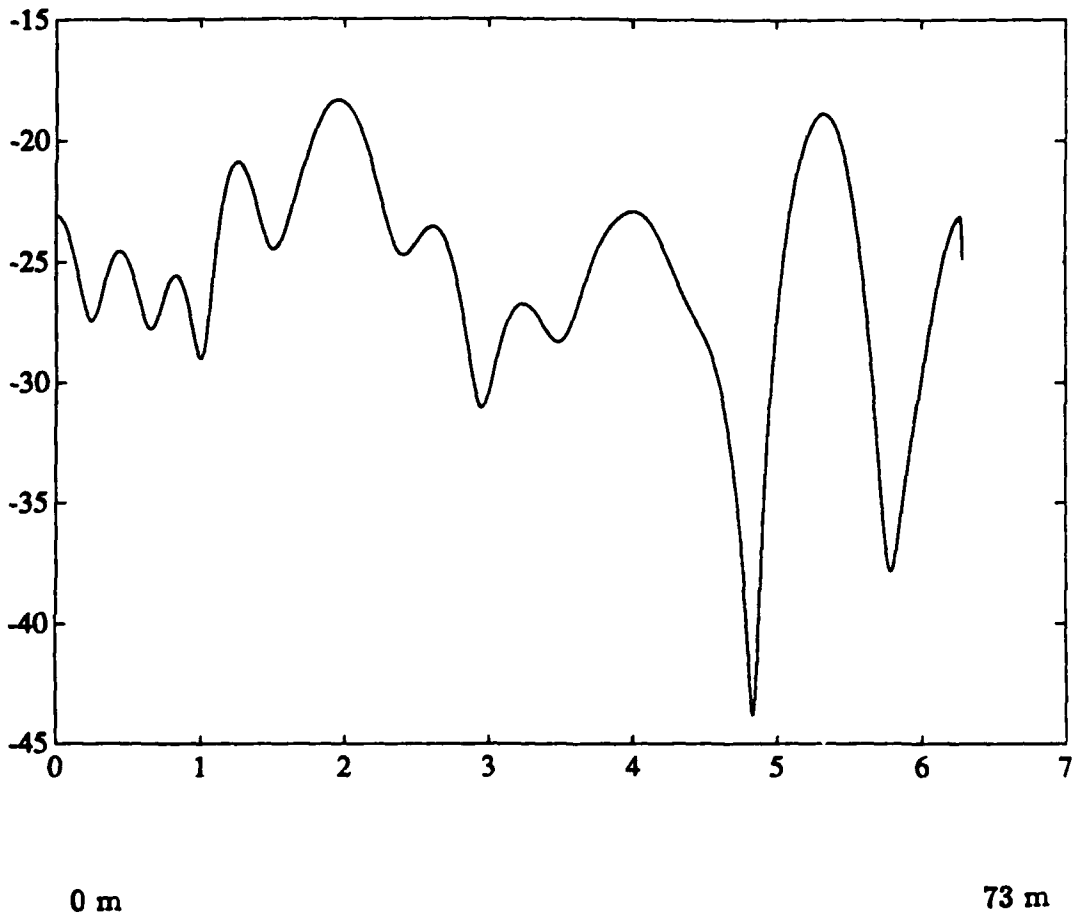

Figure 4.2: Concorde, 18-26 GHz, FFT using 30 data points zero padded to 512, 0 degree aspect angle.

tenth order model and respectively 3, 5 and 7 singular values are kept. For all three cases the threshold mentioned in Step 1b has been taken as the first large drop in the magnitude of the singular values, which occurs after the second singular value in all three cases. It can be clearly seen that the estimated zeros are very similar indeed, and the associated energies are also quite similar. If we compare this figure with Figure 4.4, in which we have dropped the model order M from ten to five, we see that the two zeros are still in the same place, although the estimated energy of the weaker scattering center differs from those in Figure 4.3. Thus we see that the algorithm presented in Table 3.1 is indeed less sensitive then the previous algorithm to the choice of model order and number of singular values kept.

If we use a properly scaled picture of Concorde, such as shown in Figure 4.5, to check for the geometric relevance of the two detected scatterers, we can see that the first peak would seem to correspond to the leading edge of the wings, and the second peak appears to correspond to the trailing edge of the wing and/or the tail assembly. Again, the FFT is provided for comparison in Figure 4.2.

Figures 4.6 and 4.7 show the response estimates for the Boeing 707. We have used $N = 30$ frequencies from 18–26 GHz (this corresponds to 67–173 MHz measurements of the unscaled target). In Figure 4.6, the model order $M = 10$, and the number of singular values kept n is 7 and 5, respectively. Note that these are the same parameter choices as made for the Concorde in Figure 4.3. In Figure 4.7, $M = 7$ and $n = 5$ sv's are kept. In all these cases the zero selection was based on the energy criterion, and 5 zeros were kept. Again, we see that the algorithm is very insensitive to changes in the parameters. The FFT data is shown in Figure 4.8

Comparing the results with Figure 4.9, a scaled picture of the Boeing 707, we

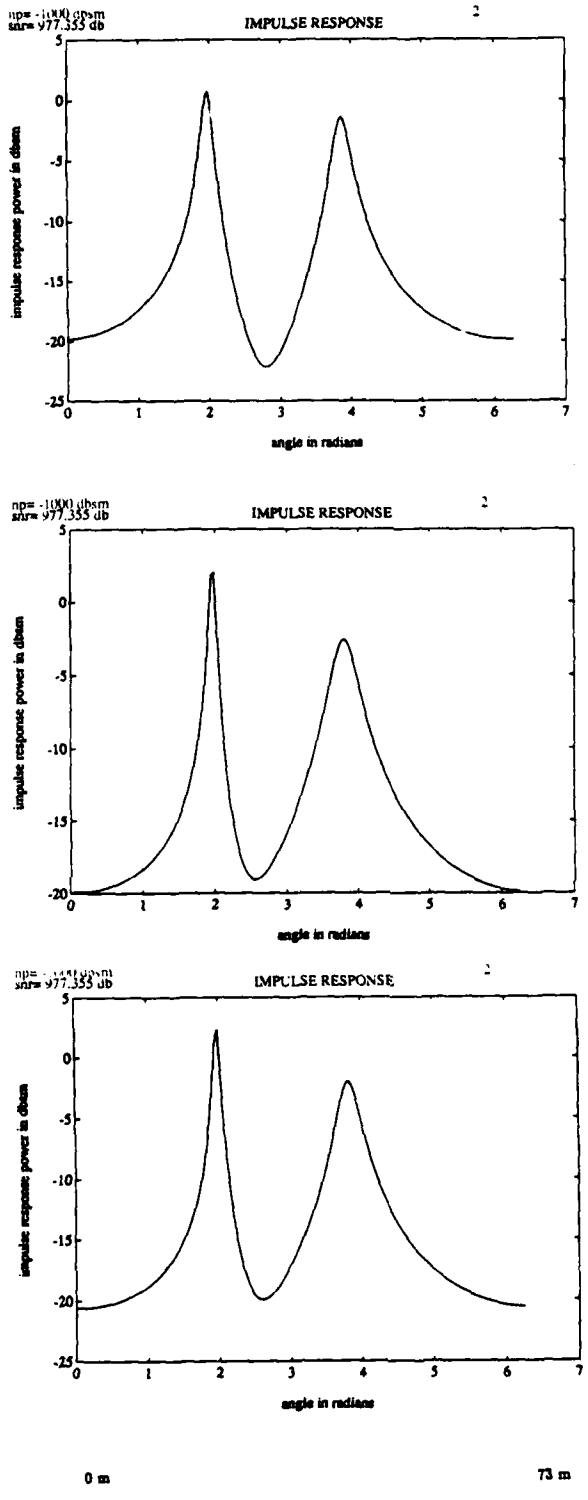

Figure 4.3: Concorde, 18-26 GHz, 10th order model, 3, 5 and 7 sv's kept, 2 zeros kept, 0 degree aspect angle.

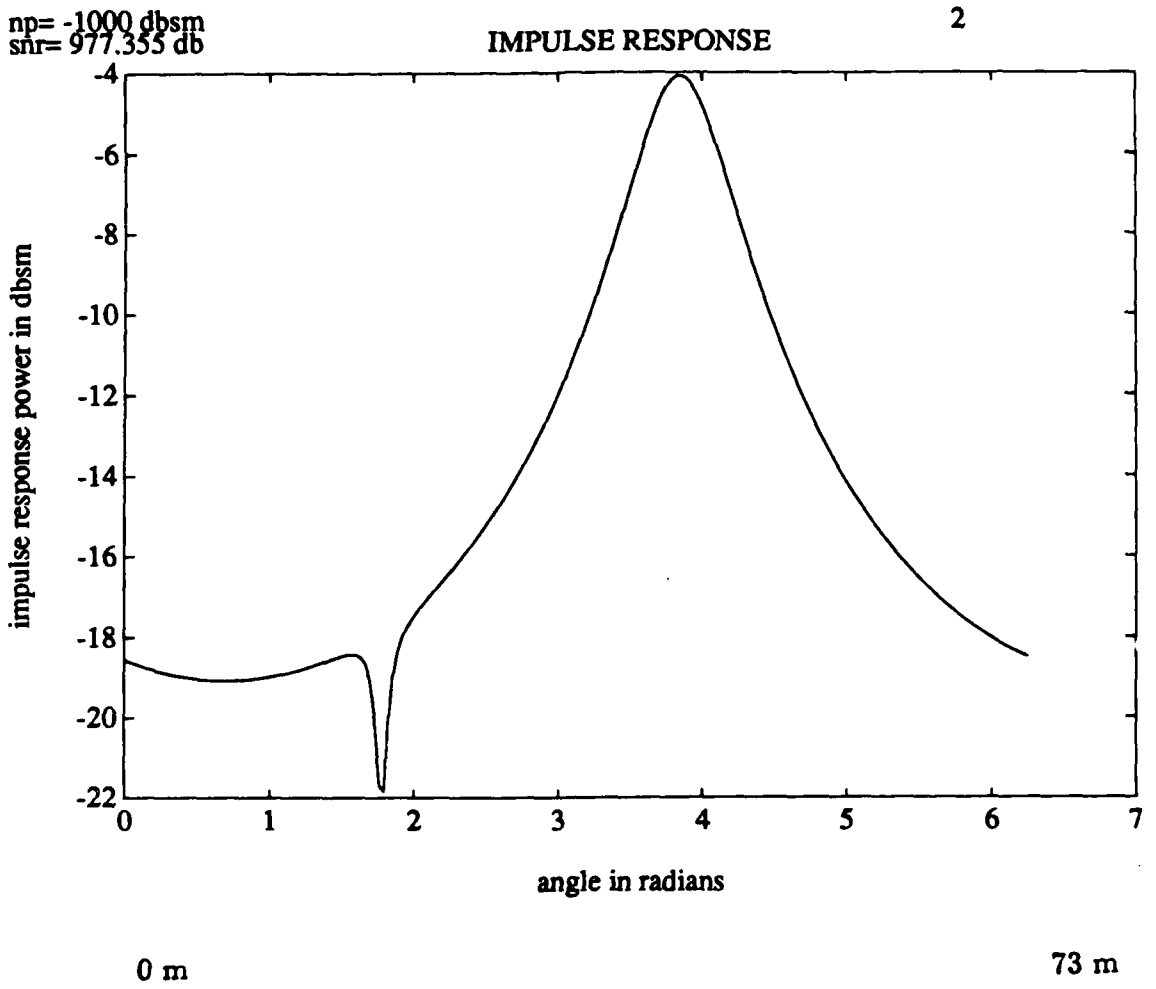

Figure 4.4: Concorde, 18-26 GHz, 5th order model, 3 sv's kept, 2 zeros kept, 0 degree aspect angle.

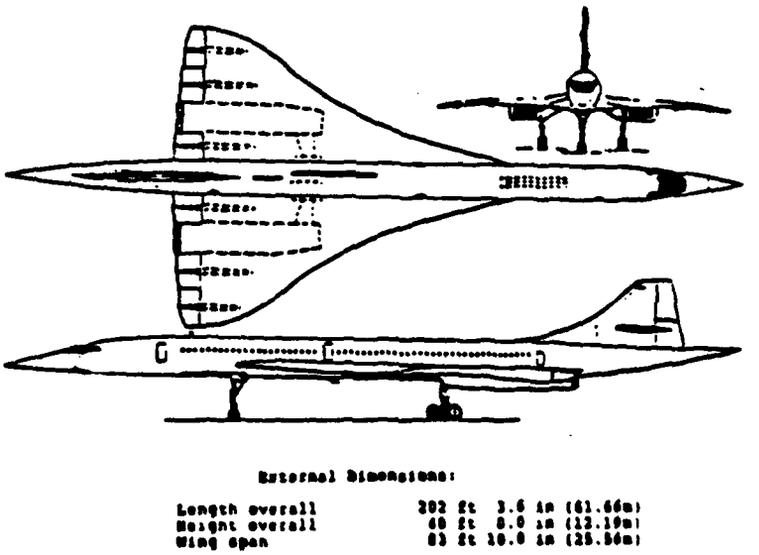

External Dimensions:

Length overall	202 ft 3.6 in	(61.66m)
Height overall	40 ft 8.0 in	(12.19m)
Wing span	83 ft 10.0 in	(25.56m)

Figure 4.5: Scaled Picture of the Concorde.

see that the middle three peaks appear to correspond to the nose, the antenna and the wing complex respectively. The two outer peaks would then be post resonances. A post resonance can appear at a smaller range than the main response because of wraparound due to range aliasing.

In summary, we have shown that the algorithm is relatively insensitive to choices of parameters. This means that a classifier based on this algorithm could operate in a robust manner. We have also shown that the estimates produced by the algorithm seem to have geometrical relevance. Finally, by comparing the results for the Concorde and the Boeing 707 we can conclude that different aircraft results in different estimates.

4.2 Tests of Performance in Noise

The above comparisons were carried out using noiseless data. This section shows that the estimates obtained are relatively insensitive to noise. We present results for the Boeing 707 and the Concorde, both at 10dB signal to noise ratio (SNR). In both cases we have used a model order $M = 7$ and kept $n = 5$ singular values. For the Concorde, we keep $m = 2$ zeros and for the Boeing 707 we keep $m = 5$.

Figure 4.10 shows the results of ten Monte Carlo simulations for the Concorde, and Figure 4.11 shows the results of the same experiment for the Boeing 707. The Figures show that the different Monte Carlo simulations lead to results that are similar both to one other and to the noiseless results (compare with Figures 4.3 and 4.6 respectively). Again, these are typical results.

Inspection of the algorithm shows that this experiment implies that the values of M and n can indeed be chosen independently of the target, since the only difference

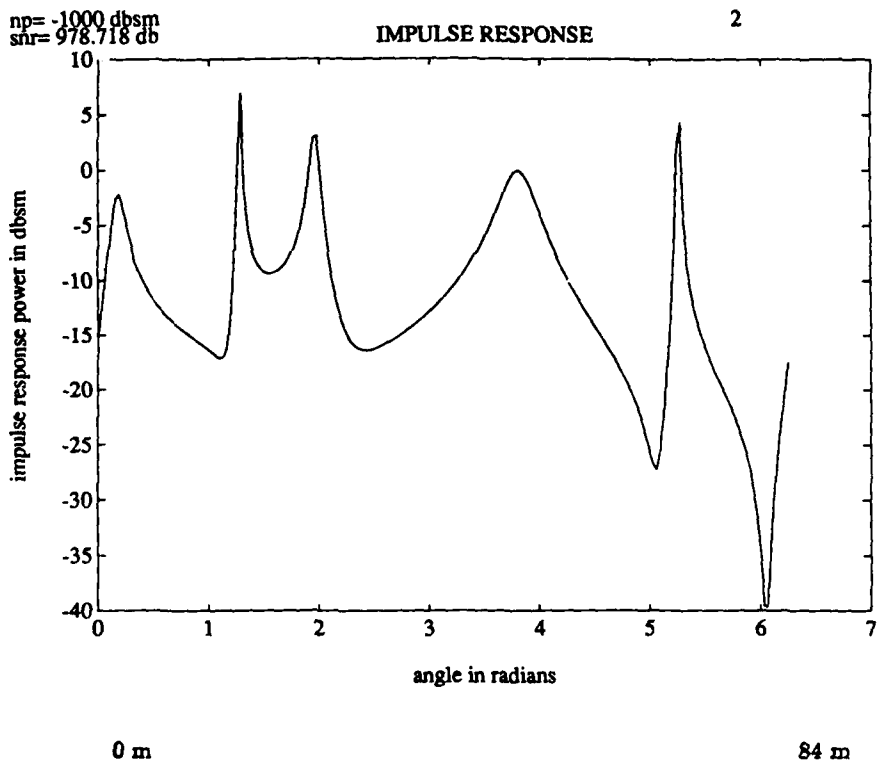

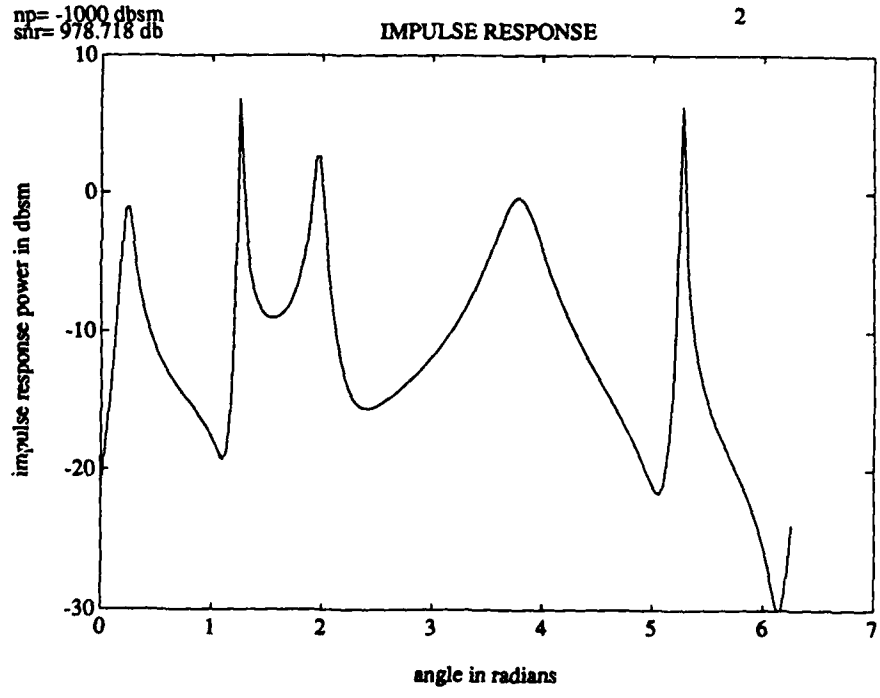

Figure 4.6: Boeing 707, 18-26 GHz, 10th order model, 7 and 5 sv's kept, 5 zeros kept, 0 degree aspect angle.

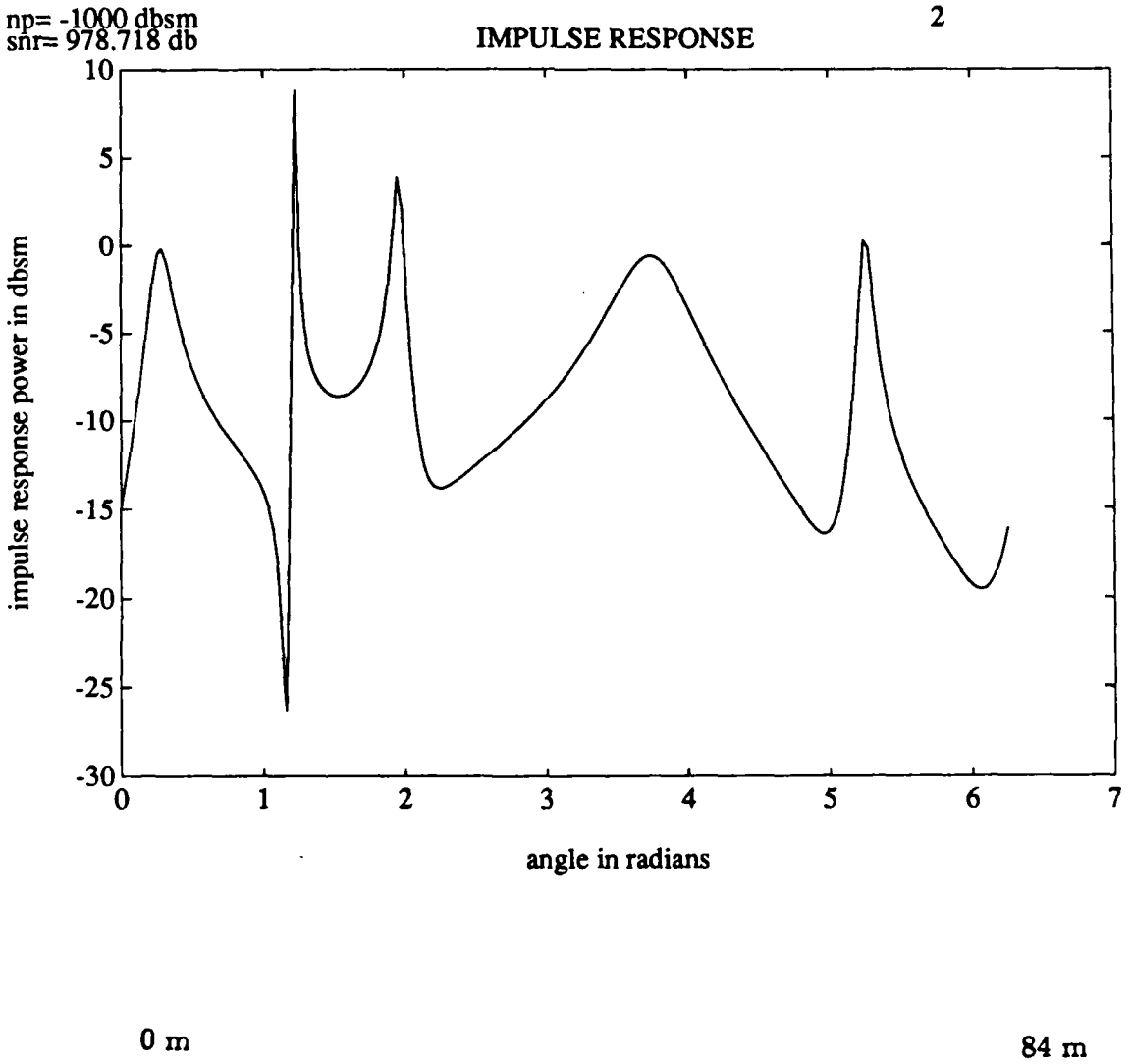

Figure 4.7: Boeing 707, 18-26 GHz, 7th order model, 5 sv's kept, 5 zeros kept, 0 degree aspect angle.

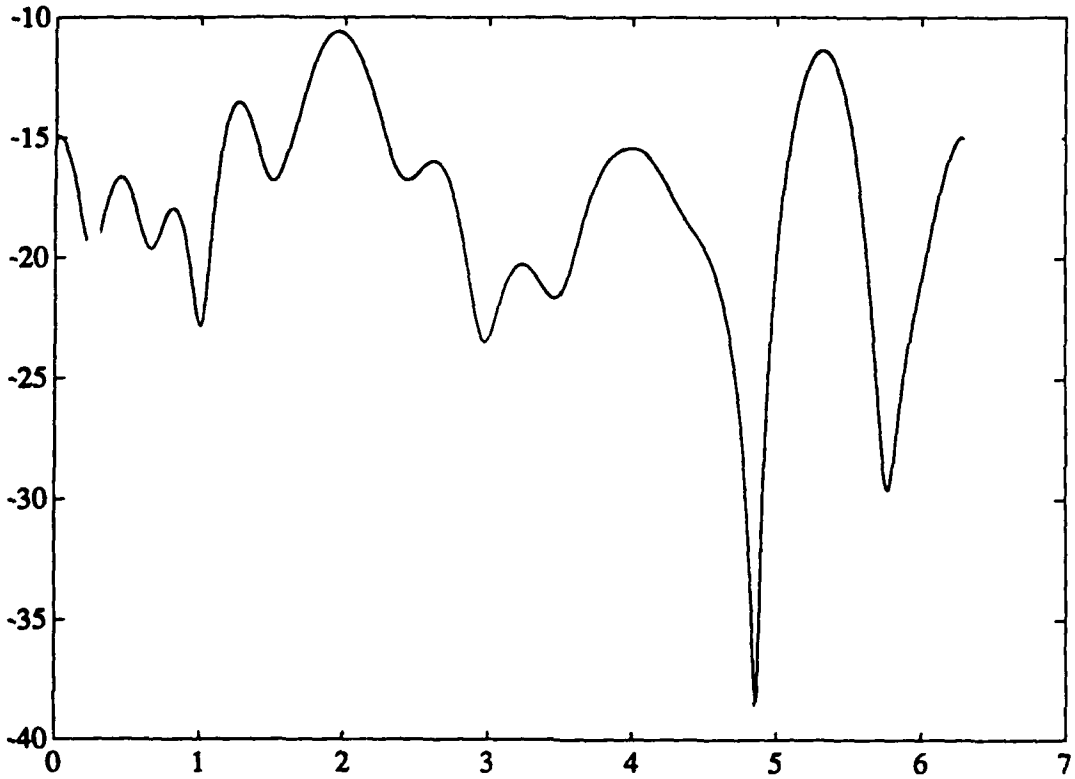

Figure 4.8: Boeing 707, 18-26 GHz, 30 point FFT zero padded to 512 points, 0 degree aspect angle.

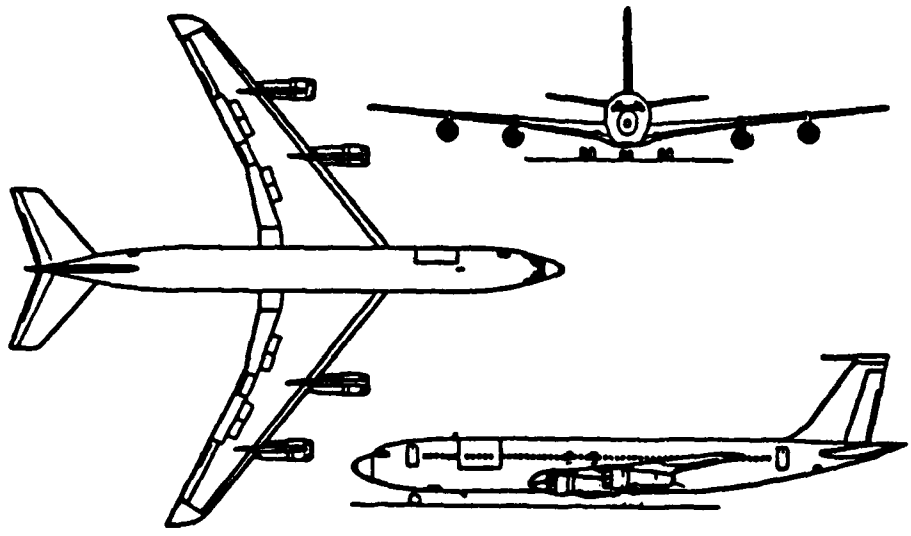

External Dimensions:

Length overall	152 ft	11.0 in	(46.61m)
Height overall	42 ft	5.0 in	(12.93m)
Wing span	145 ft	9.0 in	(44.42m)

Figure 4.9: Scaled Picture of the Boeing 707.

between the parameter values for the Concorde and the Boeing 707 is the value of m, which does not influence the choice of M or n. In fact, m can be chosen by the classification stage after the signal processing stage has run to completion. This means that the proper value of m can be made part of the data contained in the classifier's catalog.

4.3 Other Comparison Tests

This section describes some experiments showing the results of applying the algorithm to different targets, aspect angles, frequency ranges, data lengths and model orders. These results illustrate the range of applicability of the algorithm.

Figure 4.12 shows the Boeing 707 with $N = 20$ data points taken from a 6.25–12 GHz data base (this corresponds to 42–80 MHz for an unscaled target), model order $M = 10$ and number of singular values kept $n = 7$. Despite the difference in frequency range, the correspondence with Figure 4.6 is quite good (there is a difference in the position of the reference point). We see that the leftmost peak in Figure 4.6 is missing in Figure 4.12; otherwise we have similar shaped peaks occurring at the same relative spacing in both Figures.

Figure 4.13 shows the Boeing 707 with $N = 40$ data points taken from the 6.25–12 GHz range, model order $M = 10$, and $n = 7$ singular values kept. Except for the data length, these are the same choices as in Figure 4.12. Since the data length has been increased by a factor of two while keeping the bandwidth constant, the frequency step size δ_f has been halved, and hence the maximum unambiguous range R has been doubled. As a result, we expect to see the image of Figure 4.12 scaled down by half in the middle of Figure 4.13, surrounded by a flat response

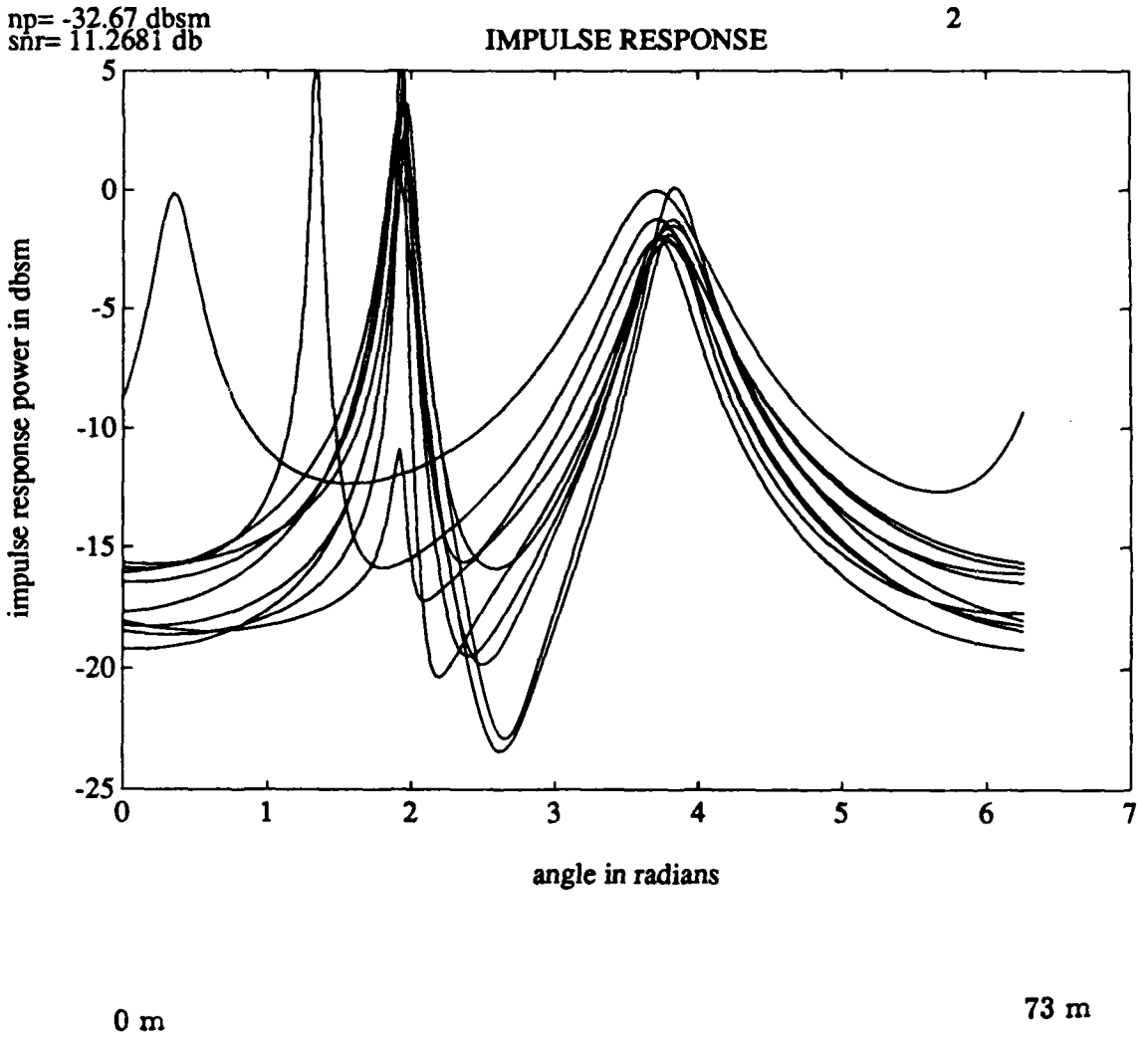

Figure 4.10: Concorde, 18-26 GHz, 7th order model, 5 sv's kept, 2 zeros kept, 10dB SNR, 0 degree aspect angle.

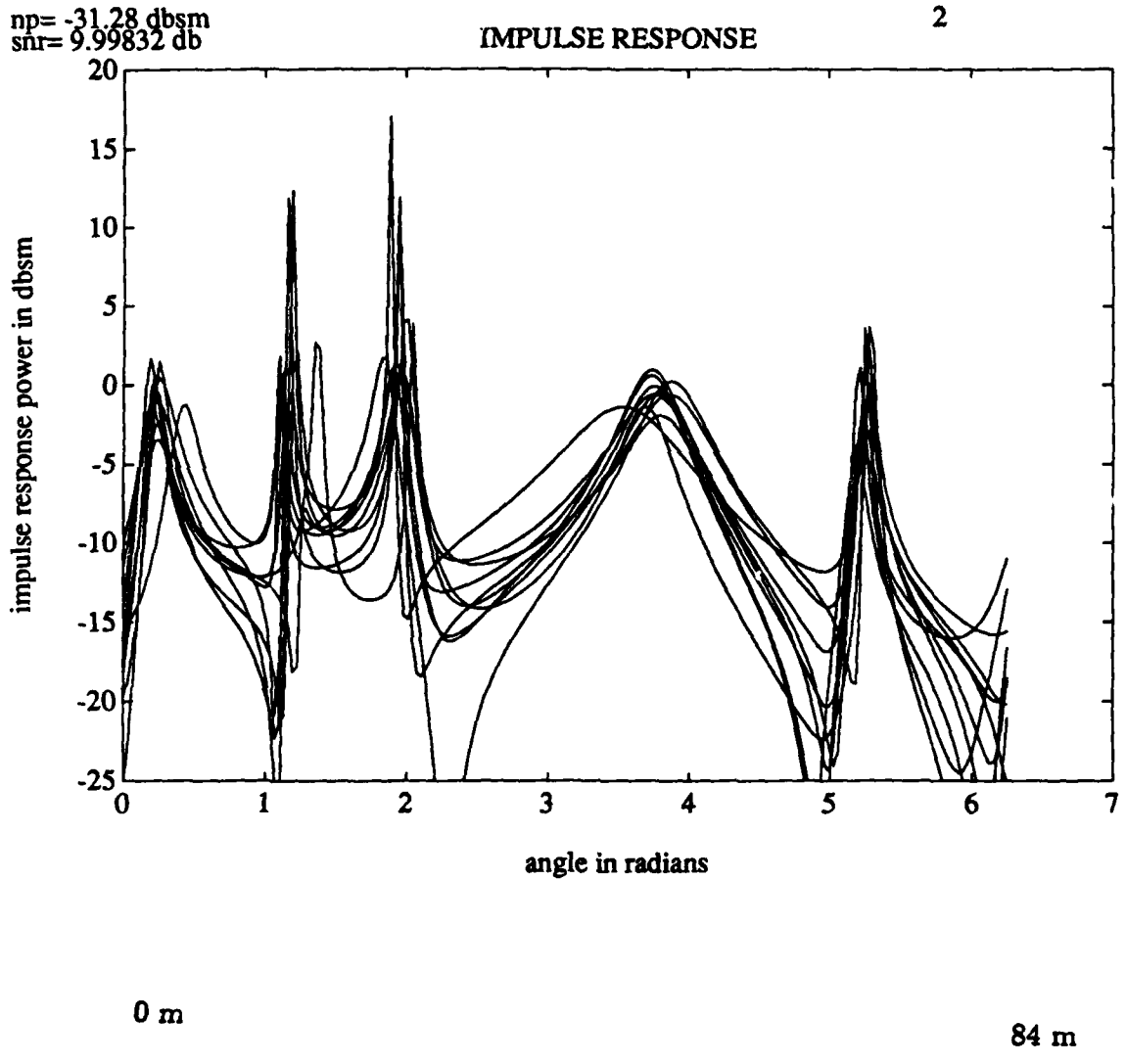

Figure 4.11: Boeing 707, 18-26 GHz, 7th order model, 5 sv's kept, 5 zeros kept, 10dB SNR, 0 degree aspect angle.

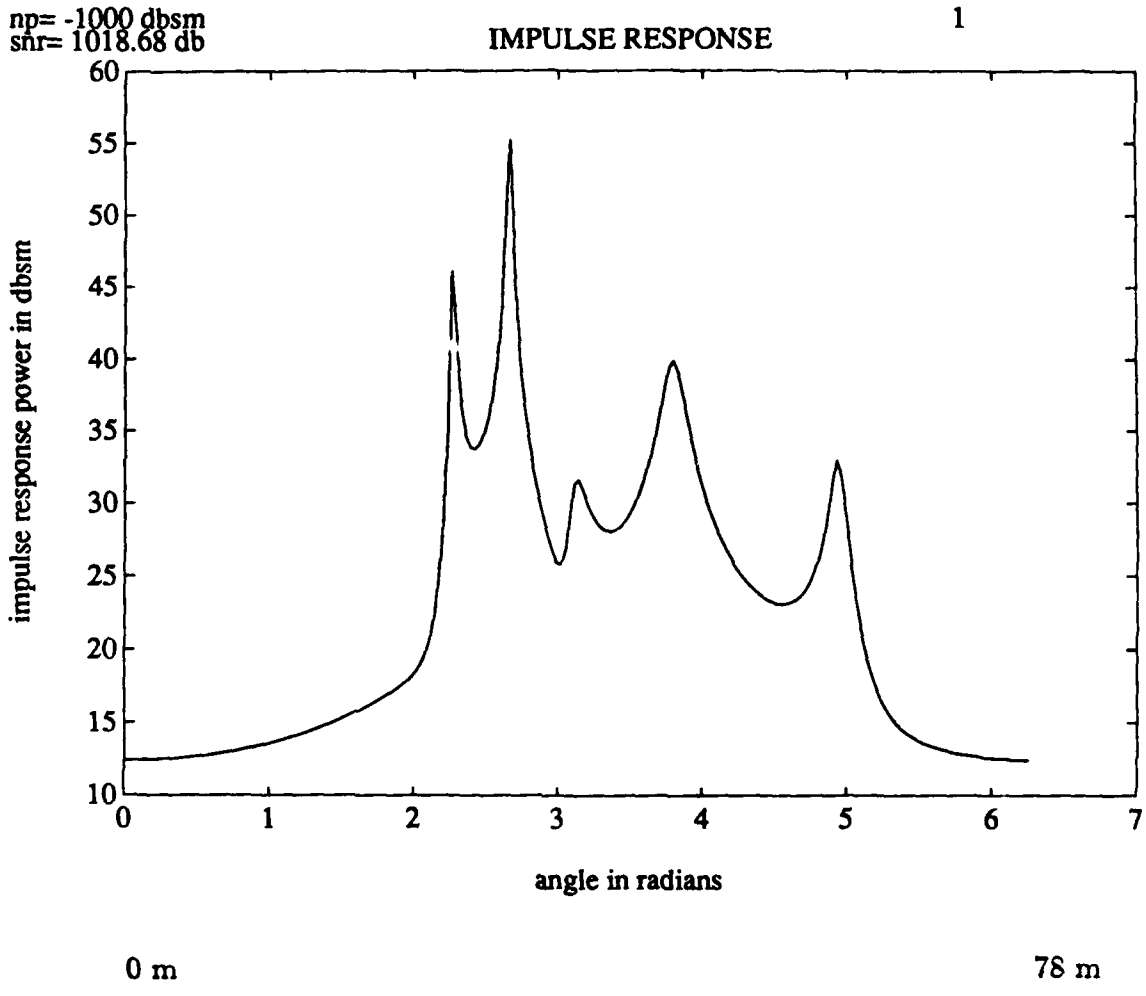

Figure 4.12: Boeing 707, 6.25–12 GHz, 20 data points, 10th order model, 7 sv's kept, 0 degree aspect angle.

indicating the absence of target. Comparing Figures 4.12 and 4.13, this is exactly what we see.

In Figure 4.14 we see the Concorde, using $N = 20$ data points from the 6.25–12 GHz range (48–92 MHz for a full-scale target), model order $m = 10$ and $n = 7$ singular values, at 0 and 20 degrees aspect angle. As can be seen from the figure, main scattering behaviour is similar. The second large peak at 0 degrees has split into two narrower peaks at 20 degrees, and all of the peaks are are a bit closer in the 20 degree plot ,due to the apparent shortening of the target in the downrange direction.

Figure 4.15 shows the DC 10 using $N = 20$ data points from 6.25–12 GHz (31–60 MHz for a full scale target) and model order $m = 10$ with $n = 10$ singular values in the one curve, and $m = 6$ and $n = 4$ in the other. Clearly, all major features are preserved despite the changes in model order and number of singular values kept. Figure 4.16 shows a scale model of the DC 10 which compares to the scale in Figure 4.15.

In summary, we see that each plane has its own characteristic response, which is preserved well through changes in frequency band, model parameters, and aspect angle. Moreover, small (20 degrees) changes in aspect angle lead to predictable, smooth changes in the response. As a result, we expect to be able to identify both target type and target aspect angle on basis of the parameters computed by this algorithm.

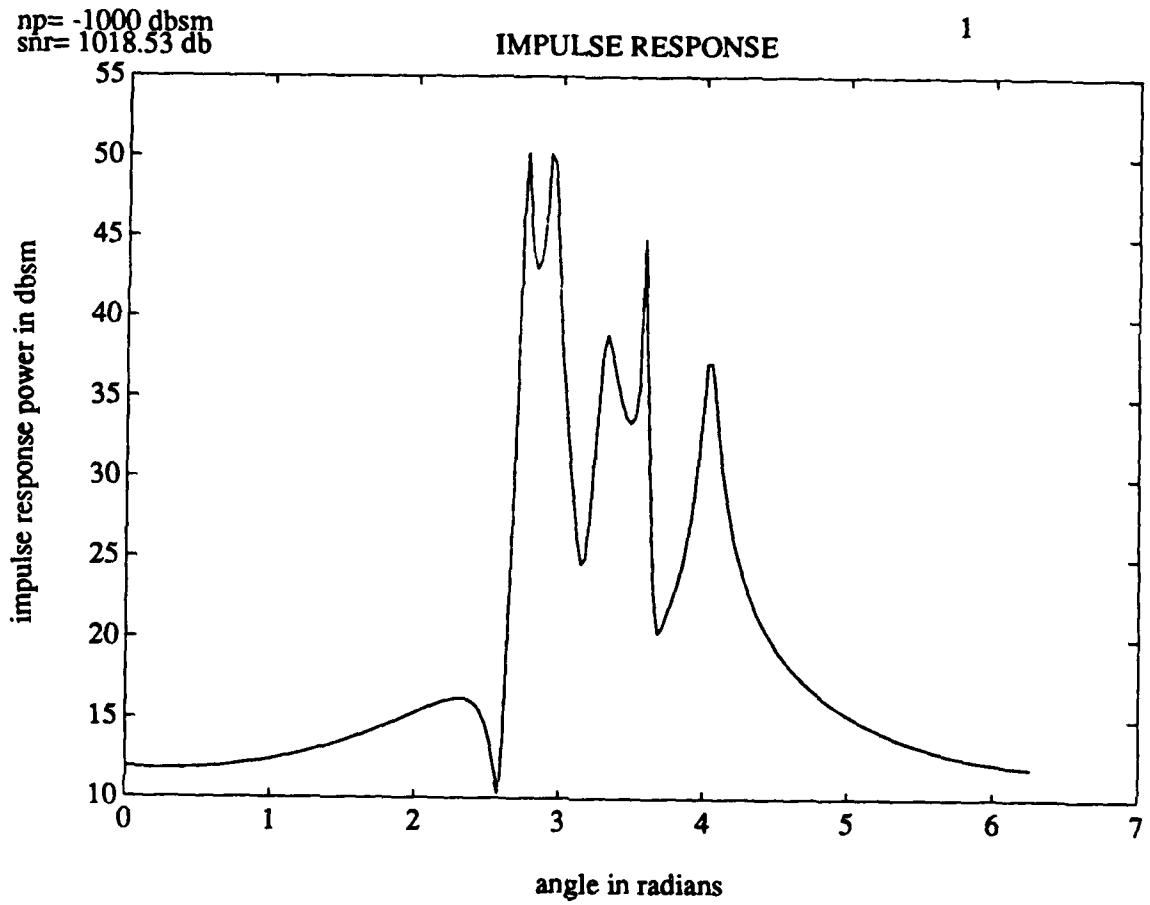

0 m

156 m

Figure 4.13: Boeing 707, 6.25–12 GHz, 40 data points, 10th order model, 7 sv's kept, 0 degree aspect angle.

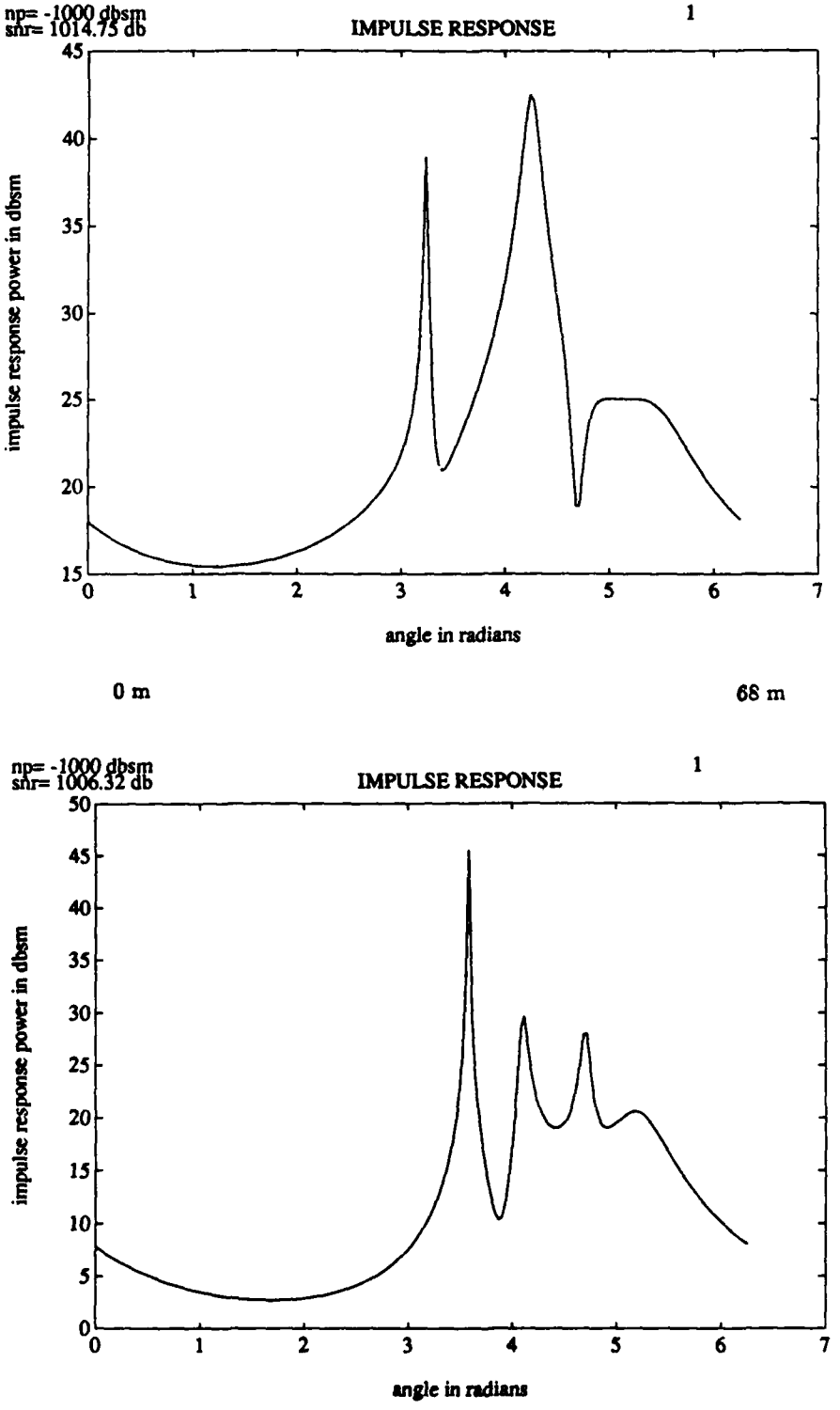

Figure 4.14: Concorde, 6.25–12 GHz, 20 data points, 10th order model, 7 sv's kept, 0 and 20 degrees aspect angle.

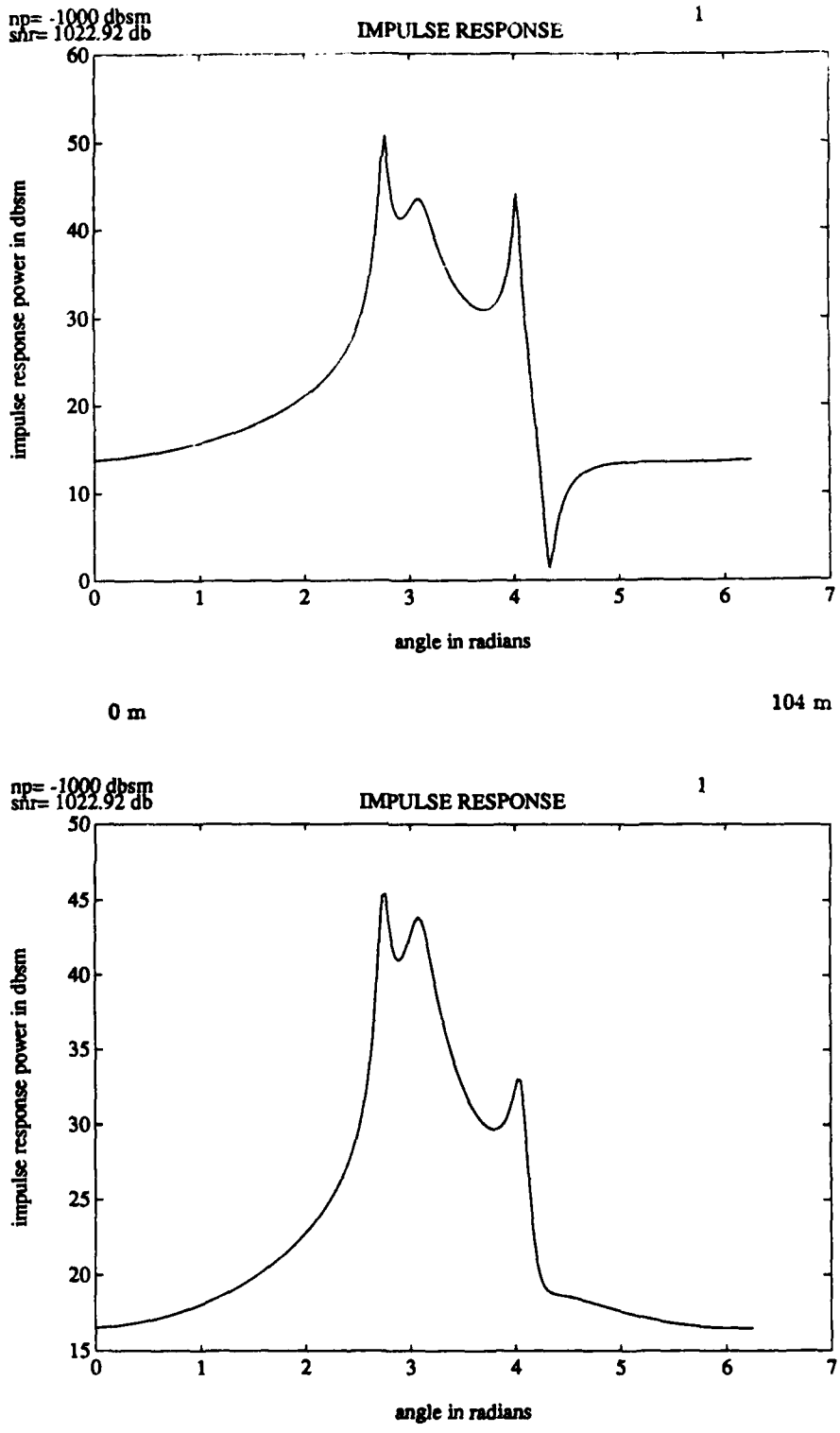

Figure 4.15: DC 10, 6.25–12 GHz, 20 data points, 10th and 7th order model, 7 and 4 sv's kept, 0 degree aspect angle.

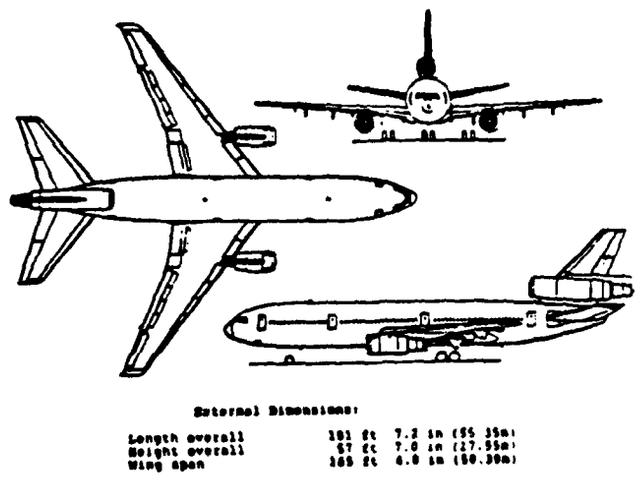

Figure 4.16: Scaled picture of the DC 10.

5. Conclusions

We have developed an ARMA algorithm suitable for the estimation of radar target responses from frequency domain data. We have shown that the algorithm is robust with respect to changes in the model parameters and to changes in the frequency band employed. We have also shown that the algorithm performs reliably in the presence of noise. Using data from the ElectroScience Laboratory Compact Range, we have shown that different targets do indeed produce different response estimates, and that varying the aspect angle of the target by a small amount (20 degrees) leads to smooth and predictable changes in the estimated response.

Since the remaining manual steps in the algorithm (the choices of the number of singular values and zeros to keep) are easily automated, we expect that the algorithm in its present form is suitable to serve as a signal processing front end for a radar target identifier. With such a configuration, we expect to be able to identify both the nature of the target and its aspect angle. This method has the advantage that the signal processing stage can serve to both transform the frequency data into geometrically relevant information and perform data compression (the number parameters output by the algorithm is less than the number of data points). This is important for the computational burden imposed by the classifier stage. The performance of such a two stage classification procedure needs to be investigated.

The algorithm itself could be improved by studying its statistical properties and the effects of unmodeled dynamics on performance. The latter is especially important in radar target applications, because the target typically contains far more scatterers than we model. In addition to this, our model is an approximation to the actual electromagnetic phenomena. It is known from empirical studies that

the singular value decomposition helps to combat the effects of noise and unmodeled dynamics, but the mechanism behind this is very poorly understood, especially for the short data length case, such as we have in the radar target problem. These problems are strong candidates for further study.

6. References

[1] D. L. Mensa, *High Resolution Radar Imaging.* Dedham, MA: Artech House, 1981.

[2] W. Leeper, "Identification of scattering mechanisms from measured impulse response signatures of several conducting objects," M.S. Thesis, The Ohio State University, 1984.

[3] R. L. Moses and R. Carrière, "Parametric modeling of radar targets using canonical scattering centers," Technical Report 719267-13, The Ohio State University, Department of Electrical Engineering, ElectroScience Laboratory, December 1988.

[4] L. Marple, *Digital Spectral Analysis with Applications.* Englewood Cliffs: Prentice-Hall, 1987.

[5] T. Kou and A. A. L. Beex, "Parameter identification of exponential signals in colored noise environments," in *8th IFAC Symposium on Identification and System Parameter Estimation*, August 27–31 1988.

[6] M. A. Rahman and K. Yu, "Total least squares approach for frequency estimation using linear prediction," *IEEE Transactions on Acoustics, Speech, and Signal Processing*, vol. ASSP–35, no. 10, pp. 1440–1454, October 1987.

[7] D. W. Tufts and R. Kumaresan, "Improved spectral resolution," *Proceedings of the IEEE*, vol. 68, no. 3, pp. 419–420, March 1980.

[8] R. Kumaresan and D. W. Tufts, "Estimating the parameters of exponentially damped sinusoids and pole-zero modeling in noise," *IEEE Transactions on Acoustics, Speech, and Signal Processing*, vol. ASSP-30, no. 6, pp. 833–840, December 1982.

[9] D. W. Tufts and R. Kumaresan, "Estimation of frequencies of multiple sinusoids: making linear prediction perform like maximum likelihood," *Proceedings of the IEEE*, vol. 70, no. 9, pp. 975–989, September 1982.

[10] R. L. Moses and R. Carrière, "Autoregressive moving average modeling of radar target signatures," Technical Report 717220-6, The Ohio State University, Department of Electrical Engineering, ElectroScience Laboratory, January 1988.

[11] A. Kamis, E. K. Walton, and F. D. Garber, "Radar target identification techniques applied to a polarization diverse aircraft data base," Technical Report 717220-2, The Ohio State University, Department of Electrical Engineering, ElectroScience Laboratory, March 1987.